Performance of surface plasmon resonance imaging system based on angular modulation and intensity measurement*

ZHANG Lu-lu (张璐璐)**, **CHEN Xing** (陈兴), **and CUI Da-fu** (崔大付)
State Key Laboratory of Transducer Technology, Institute of Electronics, Chinese Academy of Sciences, Beijing 100190, China

(Received 8 December 2015)

This paper presents a surface plasmon resonance (SPR) imaging system based on angular modulation (AM) and intensity measurement (IM) together to avoid the mechanical errors of the angle scanning device. The SPR resonant angle was found by angular scanning method and then the light intensity changes were collected at a fixed incident angle. Glycerol gradient solution (0%, 1%, 2%, 3% (weight percentage) glycerol dissolved in water) experiments were conducted, which indicate that the best fixed angle location is the middle of the linear range of SPR absorption peak and the central area signals are more uniform than those of the border areas. The sensitivity differences of different areas of SPR images are studied, and an optimized algorithm is developed.
Document code: A **Article ID:** 1673-1905(2016)03-0226-3
DOI 10.1007/s11801-016-5247-7

Surface plasmon resonance (SPR) is an optical label-free, real-time, fast and quantitative detection technology[1,2], which is the most commonly used to measure interaction of molecules. SPR reflectivity measurement is surface sensitive, which has been used to measure interactions between DNAs[3], DNA and protein[4], proteins[5-7], peptide and protein[8], protein and cells[9,10].

SPR imaging is also called SPR microscopy which was first demonstrated in 1988[11]. The most popular SPR imaging sensing scheme uses the prism coupling method of the Kretschmann and Raether configuration[12,13]. The commonly used detection approaches in SPR sensors are based on angular modulation (AM), wavelength modulation (WM) and intensity measurement (IM)[14]. The theoretical sensitivity for AM approach is a little higher[15], in which a single wavelength is used and a laser beam is incident on the metal film through the prism, scanning over the incident angles. However, the AM approach requires high accuracy and high speed scanning device, which limits the SPR sensor sensitivity.

In this paper, we combine AM and IM approaches together. Firstly, the resonant angle was found by AM method. Then the incident angle was fixed near the resonant angle and the light intensity changes were collected to computer. The sensitivity differences of different areas of SPR images were studied in the experiments. An optimized algorithm for data processing to compensate the inconformity of light intensity in the SPR imaging system was introduced.

The homemade SPR imaging system is based on the prism coupling mode of the Kretschmann structure. The coupling angle is sensitive to changes in the refractive index of the medium adjacent to the metal layer supporting surface plasmons. As shown in Fig.1, the proposed SPR imaging system consists of a red laser light source (650 nm peak wavelength), a prism with an equilateral triangle shape (n=1.72; Beijing Glass Factory, China), a glass slide coated with a gold film (50 nm in thick), and a CCD camera (Basler, A102f). The laser, the polarizing filter and the lens system were installed on a rotating arm. The CCD was mounted on the other rotating arm, and both rotating arms were controlled by a stepper motor. The incident angle was capable of changing from 40° to 70°, satisfying the needs for most biochemical detection experiments.

The SPR sensor chips were coated with 2 nm-thick chromium then 50 nm-thick gold film by magnetron sputtering technology on 20 mm×20 mm×0.3 mm ZF4 glass substrates. An S-shape polydimethylsiloxane (PDMS) flow cell was immobilized on top of the sensor chips for various biochemical reactions as shown in Fig.1. The flow cell contains an S-shape flow channel which was made by a mixture of the PDMS oligomer and the crosslinking agent (Sylgard 184) with a 10:1 ratio. The

* This work has been supported by the National High Technology Research and Development Program of China (863 Program) (No.2014AA022303), the National Basic Research Program of China (973 Program) (No.2014CB744600), and the National Natural Science Foundation of China (Nos.61571420, 31571007, 61201079 and 81371711).
** E-mail:goldfinch1031@163.com

mixture was degassed under vacuum, poured into a silanized glass mould, and then cured in an oven at 80 °C for 8 h. After the glass mould was peeled off, the PDMS flow cell with micro reaction channels was formed. The dimension of the channel is typically 1 mm in width and 2 mm in height.

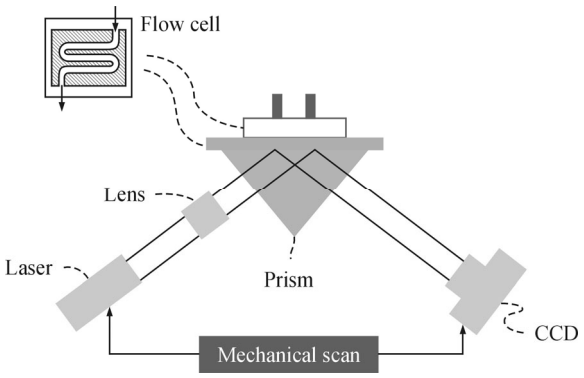

Fig.1 Schematic diagram of the SPR imaging system and flow cell

As the first step of SPR imaging characterization, gold chips were placed on top of the prism. A scan of the incident angle was first conducted in Milli-Q water to locate the absorption peak and the corresponding coupling angle. Furthermore, the incident angle was fixed near the coupling angle to measure the intensity changes of the reflected light in a dynamic real-time manner. SPR image was collected as shown in Fig.2, where 9 detection areas located in both the central and border parts of the image were selected through the software on computer. Three kinds of aqueous glycerol solutions were sequentially applied on the gold surface for system sensitivity and uniformity characterization. The location of the incident angle was changed, and the previous experiment was repeated.

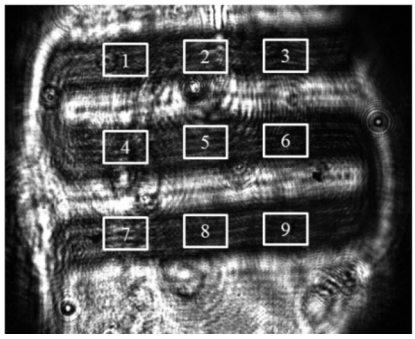

Fig.2 9 detection areas in the SPR image

Fig.3(a) shows experimental results of light intensity response unit (RU) as a function of the incident angle in Milli-Q water by scanning the incident angle from 49.8° to 57.4°, where the SPR coupling angle is 53.3°. The linear range of SPR absorption peak is from 51.7° to 52.8°. Then intensity measurement was conducted by fixing the incident angle at 5 locations (52.8°, 52.6°, 52.5°, 52.4°, 52.1°, respectively). The SPR imaging RU results to three kinds of aqueous glycerol solutions with the concentrations of 1%, 2% and 3% (weight percentage, the same below) are collected for 9 testing areas. Signals of areas 2, 4 and 5 are chosen to calculate the mean values and standard deviations for the 5 fixed locations, as shown in Fig.3(b). It is indicated that the middle of the linear range of SPR absorption peak is the best fixed angle for intensity detection, as the standard deviation value of location 4 (fixed at 52.4°) is the minimum.

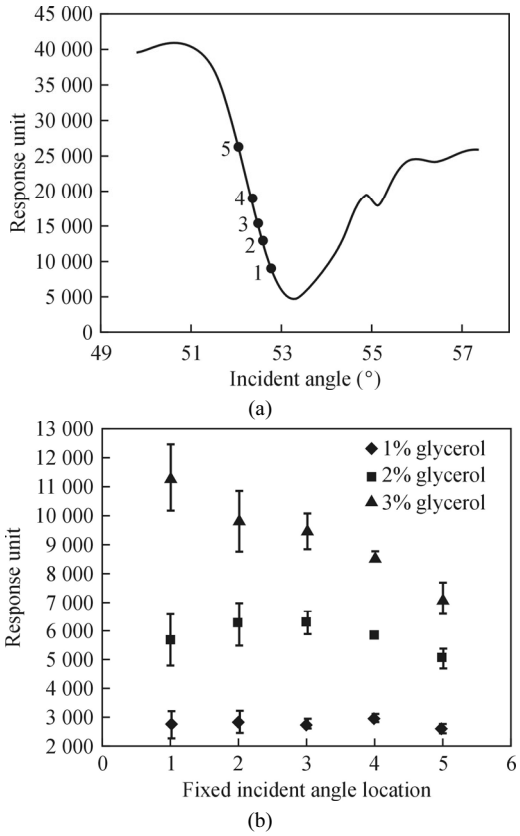

Fig.3 (a) SPR absorption peak by angle scanning from 51.7° to 52.8° (1—5 indicate the incident angles fixed at 5 locations.); (b) Mean values and standard deviations of areas 2, 4 and 5 at 5 fixed locations by detecting the glycerol gradient solutions

To compare the uniformity of different detection areas, the 9 areas are divided into 3 rows and 3 columns at the incident angle of 52.4°. The mean values and standard deviations of 3 rows are shown in Fig.4(a), and those of 3 columns are shown in Fig.4(b). The standard deviations of the columns are less than those of the rows with regard to the same detection sample. Therefore, the signals detected in the same column have a higher comparability than those detected in the same row, and also the central areas are better than the border areas.

The sensitivity difference could be reduced by calibration algorithm. Fig.5 shows the SPR signal response to refractive index of glycerol gradient solution (0%, 1%,

2%, 3% glycerol dissolved in water) for areas 4, 5 and 6 in row 2.

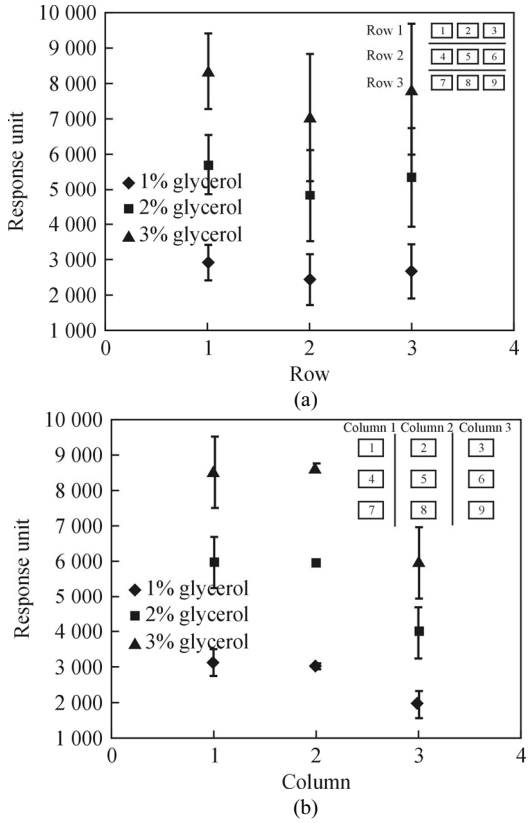

Fig.4 Mean values and standard deviations of (a) 3 rows and (b) 3 columns by detecting the glycerol gradient solutions at the incident angle of 52.4°

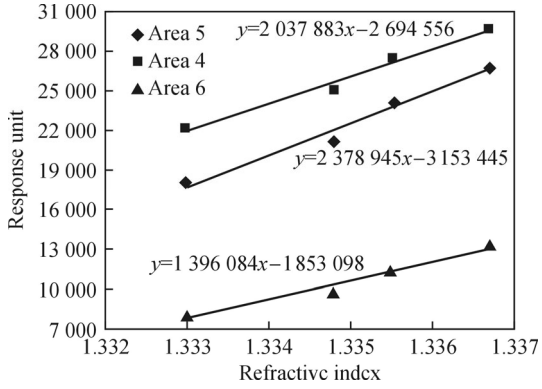

Fig.5 SPR responses to glycerol gradient solution refractive index for areas 4, 5 and 6 in row 2 and the corresponding linear fitting curves (Sample points from left to right indicate 0%, 1%, 2% and 3% glycerol dissolved in water, respectively.)

Linear fitting curves are conducted for the three areas separately with different slops (k) and intercepts (b). Linear fitting curves of areas 4 and 6 will be fitted to the linear fitting curve of area 5 where the column has higher uniformity. The fitting coefficient can be calculated as follows:

Area 5: $y = 2\,378\,945x - 3\,153\,445$;

Area 4: $y = 2\,037\,883x - 2\,694\,556$,

$k = 2\,378\,945/2\,037\,883 = 1.167\,36$,

$b = -3\,153\,445 - (-2\,694\,556) \times k = -7\,928$;

Area 6: $y = 1\,396\,084x - 1\,853\,098$,

$k = 2\,378\,945/1\,396\,084 = 1.704\,01$,

$b = -3\,153\,445 - (-1\,853\,098) \times k = 4\,252$.

The SPR signal converted into an image with the SPR imaging technique is not uniform as the light source. Development of calibration algorithm in SPR imaging sensors for data processing has received much attention lately. Calibration and optimization of the collected signal ensure that the SPR imaging system can work with better performance. In this paper, a homemade SPR imaging system is constructed by combining the AM and IM together. The middle of the linear range of SPR absorption peak is the best fixed angle location, and the central area signals are more uniform than those of the border areas. The sensitivity differences of different areas of SPR images were studied in the experiments, and an optimized algorithm was developed.

References

[1] LIU Kai-xian, Journal of Optoelectronics·Laser **26**, 199 (2015). (in Chinese)

[2] LI Zhao, YU Xian-tong, QIN Cui-fang, CAO Xiao-dan, PAN Hai-feng and XU Jian-hua, Journal of Optoelectronics·Laser **26**, 1423 (2015). (in Chinese)

[3] Piliarik M, Parova L and Homola J, Biosensors and Bioelectronics **24**, 1399 (2009).

[4] Jeong E J, Jeong Y S, Park K, Yi S Y, Ahn J, Chung S J, Kim M and Chung BH, Journal of Biotechnology **135**, 16 (2008).

[5] Li H, Cai H Y, Chen X, Sun J H, Zhang L L and Cui D F, Analytical Letters **43**, 499 (2010).

[6] Wu H, Li H, Chua F Z H and Li S F Y, Sensors and Actuators B **178**, 541 (2013).

[7] Tsai W and Li I, Sensors and Actuators B **136**, 8 (2009).

[8] Wegner G J, Wark A W, Lee H J, Codner E, Saeki T, Fang S and Corn R M, Anal. Chem. **76**, 5677 (2004).

[9] Yanase Y, Hiragun T, Kaneko S, Gould H J, Greaves M W and Hide M, Biosensors and Bioelectronics **26**, 674 (2010).

[10] Stojanović I, Schasfoort R B M and Terstappen L W M M, Biosensors and Bioelectronics **52**, 36 (2014).

[11] Rothenhausler B and Knoll W, Nature **332**, 615 (1988).

[12] Nand A, Singh V, Pérez J B, Tyagi D, Cheng Z and Zhu J, Analytical Biochemistry **464**, 30 (2014).

[13] Zhang L L, Chen X, Wei H T, Li H, Sun J H, Cai H Y, Chen J L and Cui D F, Review of Scientific Instruments **84**, 085005 (2013).

[14] Zhang H, Song D Q, Gao S, Zhang H Q, Zhang J and Sun Y, Talanta **115**, 857 (2013).

[15] Dou F Y, Wang P and Yu X L, Journal of Tsinghua University (Science and Technology) **54**, 202 (2014). (in Chinese)